# Nanostructure pervoskite ZnSnO$_3$ thin films for H$_2$S gas sensor

## R. H. Bari[1]*

[1]*Nanomaterials Research Laboratory, Department of Physics, G. D. M. Arts, K. R.  N. Commerce and M.D. Science College, Jamner 424 206, Maharashtra, India.

**Abstract:** In the present work an effort has been made to synthesize nanostrutured pervoskite ZnSnO$_3$ using spray pyrolysis techniques for efficient sensing of H$_2$S gas at lower operating temperature. Sensor structure showed a better sensing response (S ~ 530) at a relatively low operating temperature of 60 °C for 50 ppm H$_2$S gas with the short response and recovery time 19 and 27 s, respectively. Prepared thin films were characterized by X-ray diffraction (XRD), field emission scanning electron microscopy (FESEM), energy-dispersive X-ray (EDAX) spectroscopy and transmission electron microscopy (TEM). The results are discussed and interpreted.

**Keywords:** Spray pyrolysis techniques, Nanostrutured perovskite ZnSnO$_3$, H$_2$S sensor, Gas response.

## 1. Introduction

Development of fabrication methods for producing nanostructures has been a major focus in the field of nanoscience and nanotechnology. In recent years, a wide range of nanosized material have been synthesized to engineer desired properties such as chemical, electrical, mechanical and optical properties. Perovskites are mixed oxides with the general formula ABO$_3$, where A is a divalent or monovalent metal and B is a tetra- or pentavalent atom [1]. ZnSnO$_3$ (Zinc stannate) material has recently attracted much attention due to its controversial basic material properties, [2] such as its fundamental band gap. The interests in perovskite type oxides are mainly due to the easy modification of their electric properties by the selection of an adequate atom A or B [3–5]. The data on the synthesis of ZnSnO$_3$ are ambiguous and contradictory and among the large studies of materials, the details on ternary oxide systems with spinel or perovskite structure have been rarely published [6].

Now a days, significant efforts have been made to synthesize ZnSnO$_3$ thin films, include hydrothermal process [7], thermal evaporation [8], and low temperature ion exchange [9]. Owing into simplicity and inexpensiveness, the spray pyrolysis (SP) technique is a better chemical method at a lower cost for the preparation of thin films with a larger area. Also, it provides an easy way to dope any element in a ratio of required proportion through the solution medium. This method is convenient for preparing pinhole free, homogenous, smoother thin films with the required thickness [10]. During the last decade, a number of authors have employed the spray pyrolysis technique for the preparation of different kinds of nanoparticles.

A lot of work was done in the area of H$_2$S detection using semiconductor metal oxides thin films [11]. However, not much attention has been given to the fabrication of perovskites structure for detection of H$_2$S gas. There has been intensive research on improving the gas sensitivity and selectivity by controlling the particle size, nano-structures, sensing temperature, and surface.

Semiconductor metal oxides have attracted great attention in the past few years [12, 13]. At present, looking for new gas-sensing materials and developing the properties of known gas-sensing materials have become an active research field. The conductivity-type sensor using cubic $ZnSnO_3$ hierarchical shaped thin film was reported to detect $H_2S$ gas less than 50 ppm at 310 $^oC$ [7].In our previous works [2], $ZnSnO_3$ thin films prepared by a spray pyrolysis technique and discovered that the sensors exhibited sensitivity to $H_2$ gas (Gas response=112.93) at 350 $^oC$ for 1000 ppm. We reported for the first time that the nanostrutured $ZnSnO_3$ perovskite-type metal oxide semiconductor could be used as a new material for $H_2S$ gas (50 ppm) operating at low temperature.

In the present work, nanostrutured $ZnSnO_3$ thin films with volume ration of Zn/Sn was 4:6 prepared by spray pyrolysis technique and prepared thin films were characterized by XRD, FESEM, EDAX, and TEM. The crystal structure, crystallite size, grain size and constituents of elements of the nanostrutured $ZnSnO_3$ have been observed and their morphology have been reported. These nanostrutured $ZnSnO_3$ thin films were tested for sensing different conventional gases and were observed to be most selective and sensitive to $H_2S$ at operating temperature 60 $^0C$ with 50 ppm concentration.

## 2. Experimental

### 2.1. Preparation of thin films

Nanostructured pervoskite $ZnSnO_3$ films were prepared on preheated glass substrate using a spray pyrolysis technique and the experimental set up is described elsewhere [2]. 0.05 M Zinc chloride ($ZnCl_4 \cdot 5H_2O$ Purified Loba Chemie) and Stannic chloride ($SnCl_4 \cdot 5H_2O$ 99.9% pure, Aldrich Chemie) were prepared in deionised water. For spray combustion with volume ratio of Zn and Sn is (4:6) and sprayed the solution for different interval of time 10 min, 20 min, 30 min, and 40 min, respectively. The optimized values of important preparative parameters are: spray rate (9 ml/min), distance between substrate to nozzle (30 cm), to and fro frequency (14 cycle). Each solution was filled in a spray gun and was allowed to spray on heated glass substrate at constant temperature 400 $^0C$. Thus the thin films with different spray deposition time were obtained and referred as S1, S2, S3 and S4. These thin films were annealing at 500 $^0C$ in a muffle furnace for one hour in an air medium.

**Table 1: Process parameters for the spray deposition of pervoskite $ZnSnO_3$ thin films are shown in Table 1.**

| Name of the Sample | Volume ratio of Zn / Sn | | Spray deposition time (min.) | Substrate Temperature ($^0C$) | Annealing temperature ($^0C$) |
|---|---|---|---|---|---|
| S1 | | | 10 | | |
| S2 | 4 | 6 | 20 | 400 | 500 |
| S3 | | | 30 | | |
| S4 | | | 40 | | |

### 2.2. Details of gas sensing system

The gas sensing performance were carried out using a static gas chamber to sense $H_2S$ gas in air ambient and the experimental set up is described elsewhere [14]. The nanostructured $ZnSnO_3$ thin films were used as the sensing elements. Cr-Al thermocouple is mounted to measure the temperature. The output of thermocouple is connected to temperature indicator. Gas inlet valve fitted at one of the ports of the base plate. The air was allowed to pass into the glass chamber before start of every new gas exposure cycle. Gas concentration (50 ppm) inside the static system is achieved by injecting a known volume of test gas in gas injecting syringe. The conductance of the sensor in dry air was measured by means of conventional circuitary by applying constant voltage (5 V) and measuring the current by picoammeter. The conductance was measured both in the presence and absence of test gas.

The gas response (S) is defined as the ratio of change in conductance in gas to air to the original conductance in air.

$S = G_g - G_a / G_a$  ----------------------------- (1)

Where, $G_a$ = the conductance of the sensor in air
$G_g$ = the conductance on exposure of a target   gas.

## 3 Materials characterization

### 3.1 Determination of film thickness

The film thickness of the as-deposited films was measured by a well-known a weight difference method [15]. In order to measure the thickness of the thin films by using weight difference method, error and accuracy was found to be ± 5 % nm. The thickness, sample weight and sample area are related as:

$t = M/A.\rho$ ----------------------------------- (2)
Where, $M$ is the weight of the sample in $gm$,
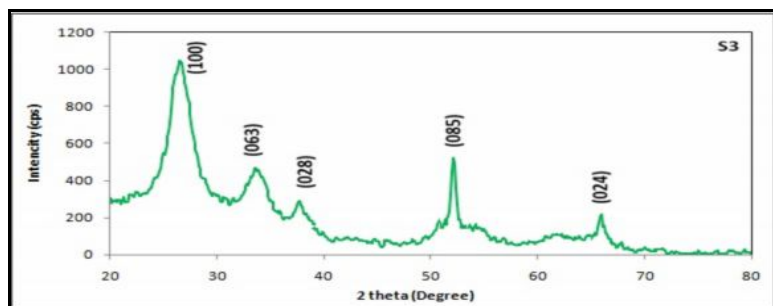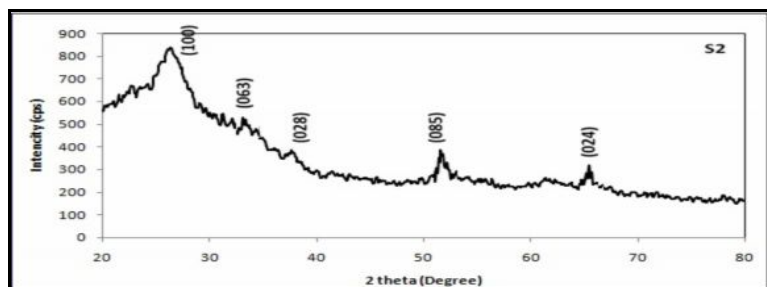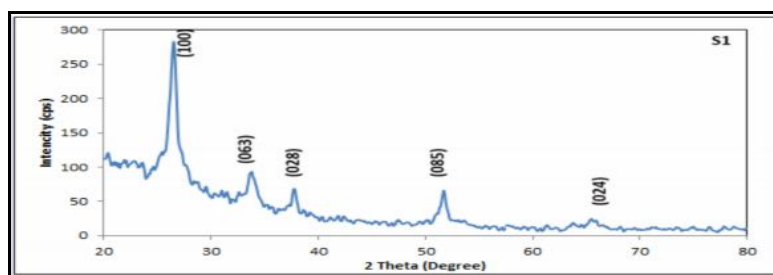A the area of the sample in $cm^2$
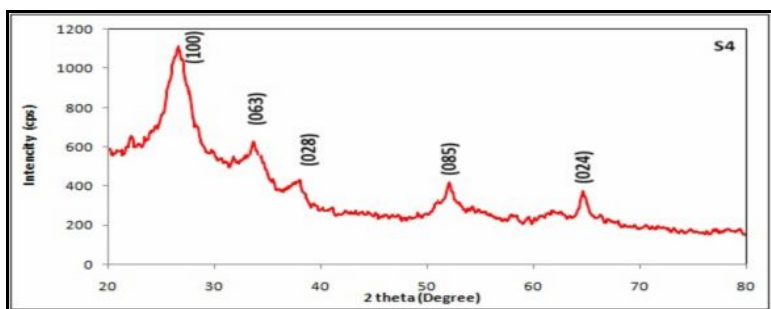and $\rho$ the materials density in $gm\,cm^{-3}$.
The values of the film thickness are given in Table 3

### 3.2. Structural analysis using XRD (X-ray diffraction)

The structural characterization of the films was carried out by analyzing the X-ray diffraction patterns (Miniflex Model, Rigaku, Japan) using CuK$\alpha$ radiation with a wavelength, $\lambda = 1\cdot5418$ Å.

**Figure 1. XRD nanostructured $ZnSnO_3$ thin films samples: S1, S2, S3 and S4**.

Fig. 1 shows the X-ray diffractogram of samples S1, S2, S3 and S4 annealing at 500 $^0$C. The diffraction peaks from various planes (100), (063), (028), (085) and (024) are matching well with standard ASTM data for perovskite $ZnSnO_3$ [16]. In the present investigation, the films exhibit a preferential orientation along the (100) diffraction plane. No diffraction peaks from any other impurities are observed. The increase of peak intensity and its sharpening indicate that the amount of the crystallite phase increases continuously with increasing spray deposition time from 10 min. to 40 min. Meanwhile, the narrowing of the width of the diffraction peak with increasing spray deposition time shows that the average crystalline size of the nano-crystals increases with increasing spray deposition time [17]. The increase in peak intensity in the diffraction pattern by increasing the spray deposition time confirms the improved crystallinity of $ZnSnO_3$ thin films. The variation of spray deposition time does not affect the preferred orientational growth of the films. But the intensity of the peak increase with spray rate. The information on the crystallite sizes of the deposited films has been obtained using Scherer's formula and it is tabulated in Table 3.

### 3.3. Elemental analysis

The quanative elemental composition and surface morphology of the spray deposited $ZnSnO_3$ thin films on glass substrate was carried out using a field emission scanning electron microscope equipped with energy dispersive spectrophotometer (FE-SEM, JEOL. JED 6300). The quanative elemental composition of $ZnSnO_3$ films was given in Table 2. Stoichiometric compositions of cations (Zn and Sn) and anions (O) are 40.00 and 60.00 at %, respectively.

**Table 2: Quantative elemental analysis of as prepared $ZnSnO_3$ thin films**

| Element | Observed at % | | | |
|---|---|---|---|---|
| | S1 | S2 | S3 | S4 |
| Zn | 23.37 | 13.09 | 10.07 | 09.18 |
| Sn | 12.49 | 16.63 | 16.17 | 16.93 |
| O | 64.16 | 70.28 | 73.21 | 73.89 |
| Total | 100.00 | 100.00 | 100.00 | 100.00 |

Table 2 indicate that the formation of and $ZnSnO_3$ films. The at % of constituents cations and anions in the pure $ZnSnO_3$ thin films are not as per the stoichiometric proportion i.e. films are nonstoichometric in nature. From table 2 it was observed that, extended spray deposition time helps to accumulate more oxygen in the structure.

### 3.4 Surface Morphology using FE-SEM

The morphology of the prepared film was analysed using a field emission scanning electron microscope (FE-SEM, JEOL. JED 6300) Figure 2(a)–(d) shows the FESEM images, showing surface topography of S1, S2, S3 and S4 thin film samples respectively. The morphology of the grains was roughly spherical in shape. The gain sizes were presented in Table 3.

(S1)

(S2)

(S3)

(S4)
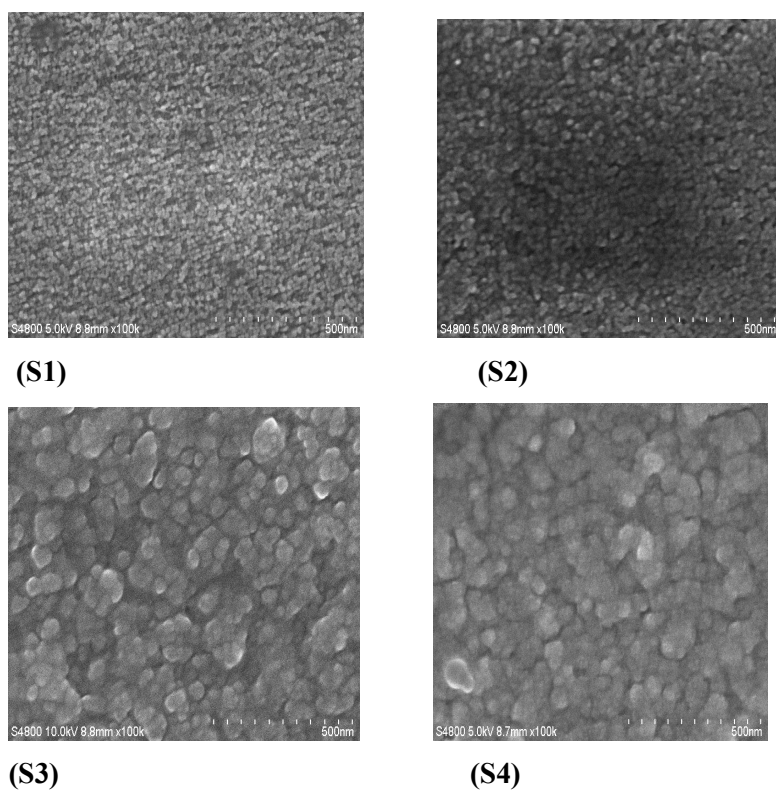
**Figure 2. FE-SEM images of prepared nanostructured drugs samples (a) S1, (b) S2, (c) S3 and (d) S4.**

### 3.5 Transmission Electron Microscopy of ZnSnO₃ thin films

Microstructure property of nanostructured $ZnSnO_3$ thin films were obtained by using transmission electron microscopy (TEM) [CM 200 Philips (200 kV HT)]



(S1)

(S2)

(S3)

(S4)
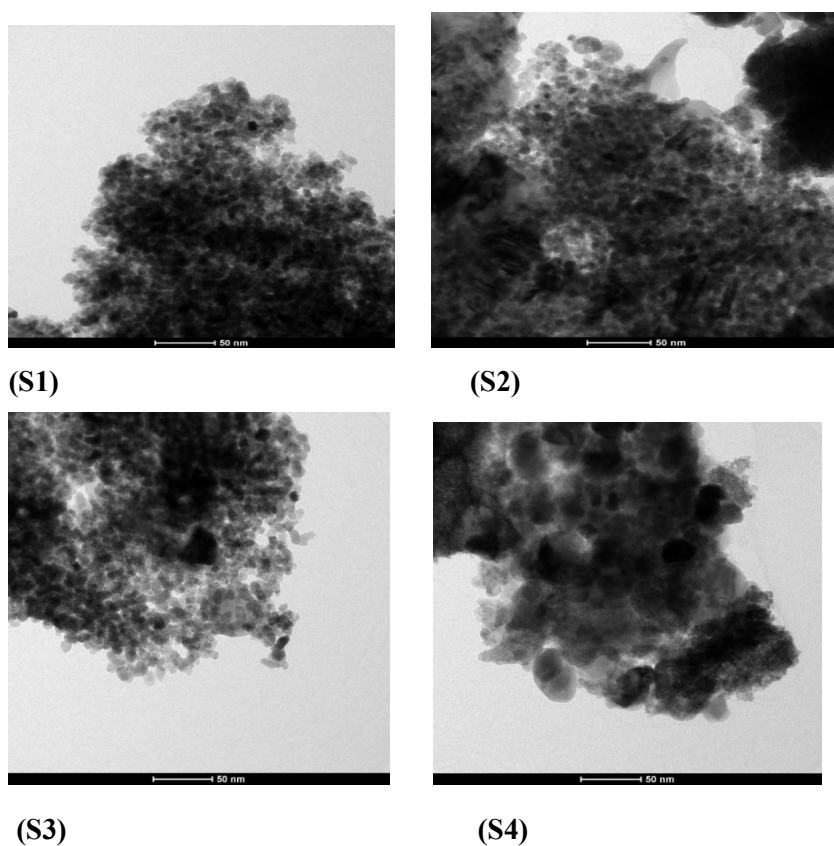
**Figure 3. TEM images of nanostructured ZnSnO₃ thin film sample: S1, S2, S3 and S4**

Figure 3 (S1), (S2), (S3) and (S4) shows the TEM images of $ZnSnO_3$ thin film sample annealed at 500 $^0C$.The grains are observed to nanocrystalline with spherical in shape. The average crystalline sizes were observed to be increased with increase in thickness of the films. The crystallite sizes were tabulated in Table 3.

**Table 3: Measurement of spray deposition time, film thickness, crystalline and grain size (from XRD, FE-SEM and TEM).**

| Sample no. | Spray deposition time (min.) | Thickness (nm) | Average crystalline size from XRD (nm) | Average grain size from FE-SEM (nm) | Average crystalline size from TEM (nm) |
|---|---|---|---|---|---|
| S1 | 10 | 223 | 11 | 16 | 11 |
| S2 | 20 | 255 | 13 | 18 | 13 |
| S3 | 30 | 330 | 16 | 19 | 16 |
| S4 | 40 | 360 | 18 | 21 | 18 |

The variation of film thickness, crystalline size (from XRD and TEM), grain size observed from FE-SEM of the deposited thin films with spray deposition time is shown in Table 3 from which, It is observed that the spray deposition time goes on increasing, the thickness of the film increases, attains 360 nm value at 40 min. (spray deposition time). At initial condition spraying time (10 min.) of the solution is low, resulting in lower thickness 223 nm.

It is clear from Table 3 that, the crystallite size, grain size calculated and observed from XRD, TEM and FE-SEM are increased with increase in film thickness. It is examined from table 3 that the crystallite size calculated from XRD match well with the crystallite size observed from TEM.

## 4. Sensing Performance of the Sensor

### 4.1 Sensing performance of $ZnSnO_3$ thin films for $H_2S$

Gas sensing performance was measured using a static gas sensing system at various concentration with different operating temperature. Gas response profiles with operating temperature to $H_2S$ are represented in Fig. 4. Sensor was observed to be most sensitive (S = 530) to $H_2S$ (50 ppm). The gas response increased with the temperature, reached to its maximum (S3=530) at 60 $^o$C and then decreased with further increase of temperature (Fig. 4).The nature of response profile in Fig. 4 may be explained as follows.
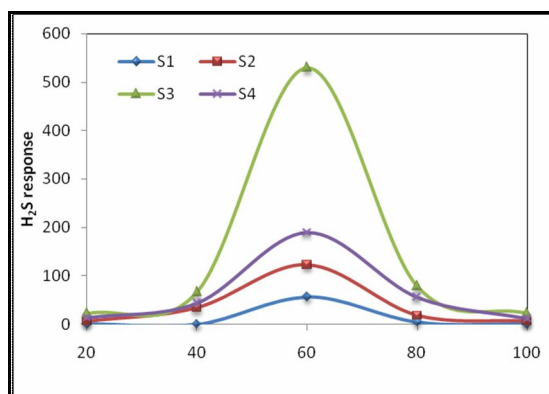


**Figure 4. Variation in response to $H_2S$ gas (50 ppm) with operating temperature**

Magnitudes of sensitivities at low and high temperatures are low while sensitivity is high at some optimum temperature between the two extremes. At lower temperatures (below 60 $^o$C), there may be stronger oxygen diffusion but smaller number of oxygen ion adsorption and hence weaker oxidizing ability of target gas. At higher temperature (above 60 $^o$C), there may be weaker oxygen diffusion toward sensor surface hence smaller number of oxygen ion adsorption – weaker oxidizing ability of target gas and poorer sensitivity. At optimum temperature of 60 $^o$C, both gas diffusion and reactivity are expected to be optimum and therefore the sensor shows maximum gas response [18].

**4.2. Effect of thickness on gas sensing performance**

Fig. 5 shows the dynamic gas response of nanostructured $ZnSnO_3$ films of different thicknesses upon exposure to 50 ppm $H_2S$ at 60°C. The maximum response was obtained with film S3 (330 nm thickness).
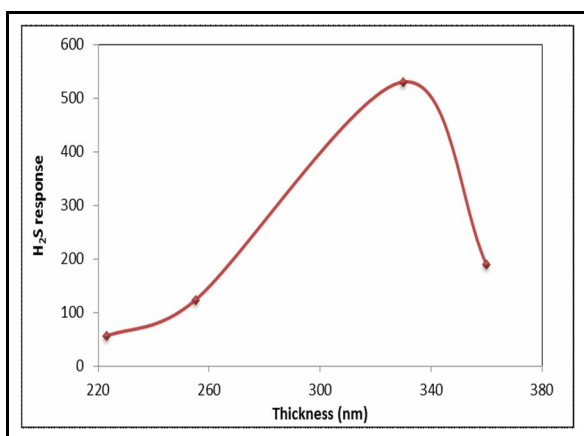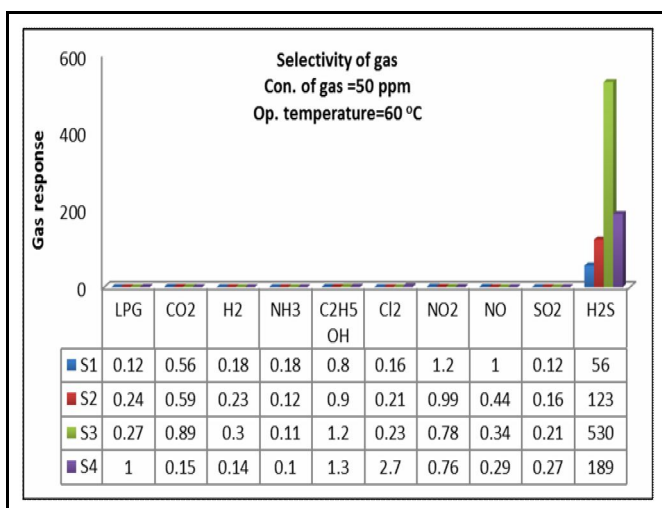


**Figure 5. Variation of films thickness with $H_2S$ gas response**

At the smaller and larger thickness sample S1 (223 nm thickness), S2 (255 nm thickness) and S4 (360 nm) gas response was low. As we know that the resistance of sample increases with an increase in thickness, through the exposure area of samples is the same, the width of potential barrier and the resistance both increased. The increase in resistivity causes the gas response decrease [19].

**4.3. Selectivity of $H_2S$ against various gases**

Selectivity is another important parameter of gas sensors. Selectivity or specificity is defined as the ability of the sensor to respond to certain gas in the presence of the other gases [20]. Selectivity of $ZnSnO_3$ thin film sensors is measured at an operating temperature of 60 °C.



Selectivity of gas
Con. of gas =50 ppm
Op. temperature=60 °C

| | LPG | CO2 | H2 | NH3 | C2H5 OH | Cl2 | NO2 | NO | SO2 | H2S |
|---|---|---|---|---|---|---|---|---|---|---|
| S1 | 0.12 | 0.56 | 0.18 | 0.18 | 0.8 | 0.16 | 1.2 | 1 | 0.12 | 56 |
| S2 | 0.24 | 0.59 | 0.23 | 0.12 | 0.9 | 0.21 | 0.99 | 0.44 | 0.16 | 123 |
| S3 | 0.27 | 0.89 | 0.3 | 0.11 | 1.2 | 0.23 | 0.78 | 0.34 | 0.21 | 530 |
| S4 | 1 | 0.15 | 0.14 | 0.1 | 1.3 | 2.7 | 0.76 | 0.29 | 0.27 | 189 |

**Figure 6. Selectivity of $ZnSnO_3$ thin films to different gases**

As shown in Fig. 6, the responses of $ZnSnO_3$ sensor to 50 ppm different gases were tested at 60 °C. It can be seen that the response of the sensor to $H_2S$ gas is much higher than to other test gases. The results show that nanostructured $ZnSnO_3$ thin films has a high selectivity to $H_2S$ at low operating temperature.

## 4.4. Variation of gas response with gas concentration
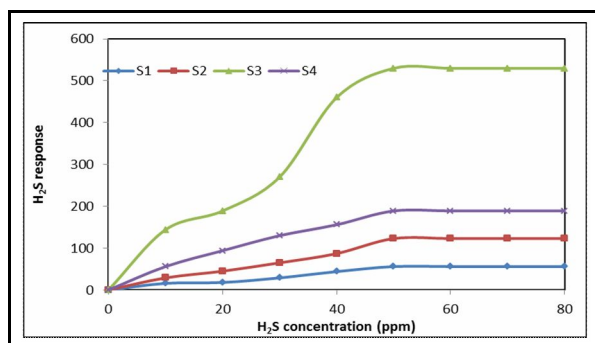


**Figure 7. Variation in gas response with H$_2$S gas concentration**

To test the H$_2$S gas concentration characteristics, the sensor was exposed to H$_2$S gas of different concentrations at a constant operating temperature. The sensor responses to H$_2$S in concentration range (10-80 ppm) are shown in figure 7 at 60 $^o$C operating temperature. The response values were observed to increase continuously with increasing the gas concentration up to 50 ppm.

The rate increase of response was relatively larger up to 50 ppm and then saturates after 50 ppm. Furthermore, we observe saturation of the sensors after exposing them to more than 50 ppm of H$_2$S gas (Fig.7), which means that no more active sites were available to react with new H$_2$S molecules when the concentration of H$_2$S was increased [21]. Thus the active region of the sensor would be between 10-50 ppm.

## 4.5. Response and recovery time
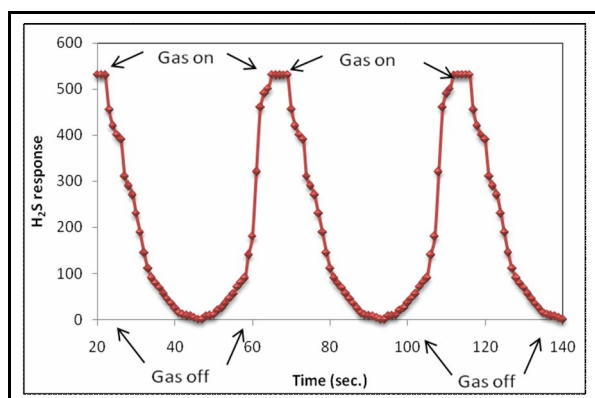


**Figure 8. Response and recovery of the sensor (most sensitive sample= S3).**

Fig. 8 shows the response and recovery characteristics of ZnSnO$_3$ thin film sensor to 50 ppm. The response of ZnSnO$_3$ thin film sensor was found to be quick (~ 19 S) to 50 ppm of H$_2$S, while the recovery was fast (~ 27 s). The fast response may be attributed to faster oxidation of the gas. The negligible quantity of the surface reaction product and its high volatility explains its fast response and quick recovery to its initial chemical status.
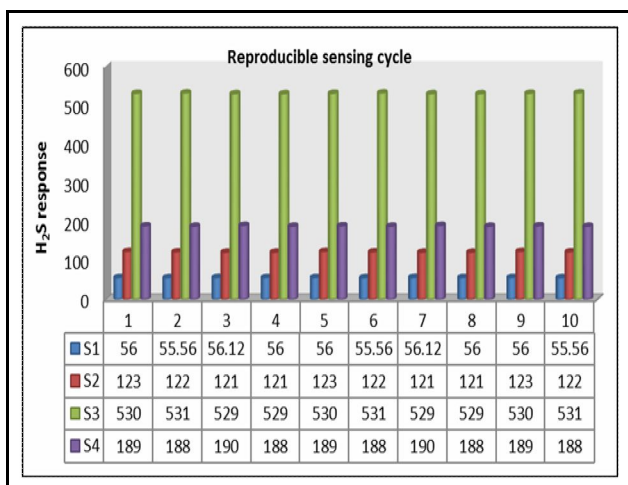
### 4.6. Stability of sensor
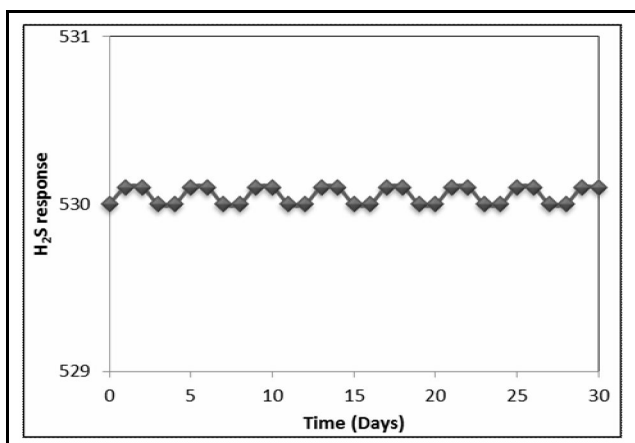


**Figure 9. The long term stability studies for nanostructured ZnSnO₃ (most sensitive sample=S3) thin film at an operating temperature of 60 °C.**

The stability of the nanostructured *ZnSnO₃* sensor were measured by repeating the test many times (30 days). During the test, no significant variation was observed as shown in Fig. 9. The H₂S gas sensor had prominent long term stability in atmosphere for about 30 days. The obtained results show that both H₂S gas response and electrical conductance were reproducible [22].

### 4.7. Reproducible sensing cycles of ZnSnO₃ thin films (S1, S2, S3 and S4)

Reproducible behaviour of each sample was tested by conducting 10 similar cycles of gas sensing process. The H₂S gas response values of each sample was observed to be approximately similar as shown in Figure 10.



| | 1 | 2 | 3 | 4 | 5 | 6 | 7 | 8 | 9 | 10 |
|---|---|---|---|---|---|---|---|---|---|---|
| S1 | 56 | 55.56 | 56.12 | 56 | 56 | 55.56 | 56.12 | 56 | 56 | 55.56 |
| S2 | 123 | 122 | 121 | 121 | 123 | 122 | 121 | 121 | 123 | 122 |
| S3 | 530 | 531 | 529 | 529 | 530 | 531 | 529 | 529 | 530 | 531 |
| S4 | 189 | 188 | 190 | 188 | 189 | 188 | 190 | 188 | 189 | 188 |

**Figure 10. Repetition of H₂S gas response for samples S1, S2, S3 and S4 at 60 °C.**

### 5. Discussion

On the basis of this sensing mechanism, it can be seen that the sensitivity of the semiconductor metal-oxide is strongly related to the charge transfer dynamics between the target gas molecules and the oxide matrix. One effective approach to improve the sensitivity of the semiconductor metal-oxide is to deposit metal nanoparticles onto the metal-oxide surface. Due to the presence of nanoparticles, the spillover effect is accelerated through "chemical sensitization" mechanism [23, 24].
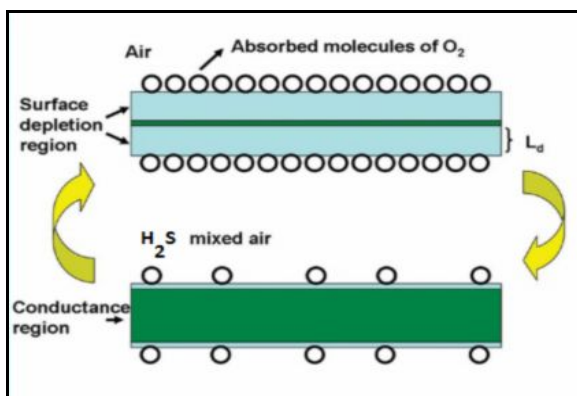
**Figure 11. Sensing mechanism of nanostructured ZnSnO₃ to H₂S gas.**

Specifically, nanoparticles can act as electron sinks because of large Helmholtz double-layer capacitance. When metal nanoparticles are deposited on a reducible oxide surfaces, partial charge transfer might occur from the center of oxide metal to the nanoparticles, leading to a negative charge accumulation on the nanoparticle surface.

This could facilitate the dissociative adsorption of oxygen onto the particle surface and consequently enhance the formation of the electron depleted layer. Additionally, the deposition of metal nanoparticles onto the oxide surface, and hence the intimate interfacial contacts, may lead to the formation of structural defects which could serve as active surface sites for the adsorption of oxygen and target gas molecules.

When the sensor is exposed to $H_2S$ gas, the $H_2S$ molecules are oxidized by oxygen species and simultaneously the depleted electrons are feedback in to particles (Shown in fig.11), resulting in an arrowed depletion layer and therefore the sensor resistance is decreased. When gas is out, the sensor will be exposed to air again and thus refreshed by air at elevated temperature. The oxygen in atmospheric air will renewably capture electrons to deplete the particle surface.

## 6. Conclusions

1. Nanostructured perovskite $ZnSnO_3$ thin films could be prepared by simple and inexpensive spray pyrolysis technique. As-deposited perovskite $ZnSnO_3$ thin films were found to be strongly adherent to the substrate.
2. Thickness of the films, crystallite size and grain size observed to increase with increase in spray rate.
3. Elemental analysis confirmed that the as-prepared $ZnSnO_3$ thin films are nonstoichiometric in nature.
4. Perovskite $ZnSnO_3$ exhibits a much higher response at low temperature and shorter response and recovery times.
5. The films may be useful for the fabrication of low operable temperature sensor.
6. Nanostructured $ZnSnO_3$ thin films showed repeatable and stability gas sensing performance.

## Acknowledgements

## References

1. Chen Z.X., Chen Y., Jiang Y.S., Comparative study of $ABO_3$ perovskite compounds. 1. $ATiO_3$ (A = Ca, Sr, Ba, and Pb) perovskites, J. Phys. Chem. B, 2002, 1069, 9986-9992.
2. Patil L.A., Pathan I.G., Suryawanshi D.N., Bari A.R., and Rane D.S., Spray pyrolyzed $ZnSnO_3$ nanostructured thin films for hydrogen Sensing, Procedia Materials Science, 2014, 6, 1557 – 1565.
3. Mao Y., Banerjee S., Wong S. S., Large-scale synthesis of single-crystalline perovskite nanostructures, J. Am. Chem. Soc. , 2003,125, 15718-15719.

4.  Hill N.A., Why Are There so Few Magnetic Ferroelectrics, Journal of Physical Chemistry, 2000,104, 6694-6709.
5.  Mahanubhav M.D., Patil L. A., Studies on gas sensing performance of CuO-modified $CdIn_2O_4$ thick film resistors, Sensor and Actuators B, 2007,128,186–192.
6.  Hotovy I., Bue D., Hascik S., Nennewitz O., Characterization and gas-sensing properties of nanocrystalline iron(III) oxide films prepared by ultrasonic spray pyrolysis on silicon, Vacuum, 1998, 50, 41-44.
7.  Zeng Yi, Zang Kan, Wang Xingli, Sui Yongming, Zou Bo, Zheng Weitao, Zou Guantian, Rapid and selective $H_2S$ detection of hierarchical $ZnSnO_3$ nanocages, Sensors and Actuators B: Chemical, 2011,159,245–250.
8.  Shen Y. S., Chang Y. S., Preparation, structure gas sensing properties of ultramicro $ZnSnO_3$ powder, Sensor and Actuators B, 1993,12, 5–9.
9.  Kovacheva D., Petrov K., Preparation of crystalline $ZnSnO_3$ from $Li_2SnO_3$ by low-temperature ion exchange, Solid state Ionics, 1998, 109,327-332.
10. Patil P. S., Versatility of spray pyrolysis technique, Material Chemistry and Physics, 1999, 59, 185-198.
11. Yamazoe N., Toward innovations of gas sensor technology, Sensor and Actuators: Chem., 2005, 108, 2-14.
12. Miyata T., Hikosaka T., Minami T., High sensitivity chlorine gas sensors using multicomponent transparent conducting oxide thin films, Sensor and Actuators B, 2000,69, 16–21.
13. Ho K.Y., Masaru Miyayama, Hirooki Yanagida, $NO_x$ gas responding properties of $Nd_2CuO_4−y$ thick film, Mater. Chem. Phys., 1997, 49, 7–11.
14. Bari R.H., Khadayate R.S., Patil S.B., Bari A.R., Jain G.H., Patil L.A., Kale B.B., Preparation, characterization and $H_2S$ sensing performance of sprayed nanostructured $SnO_2$ thin films, ISRN Nanotechnology, 2012,734325, 1-5.
15. Bari R. H., Patil S.B., Pervoskite nanostructured $CdSnO_3$ thin films as $Cl_2$ gas sensor operable at room temperature, Sensor letters, 2015, 13, 1–10.
16. JCPDS data card no. 28-1486.
17. Amma D. S. D., Vaidyan V.K., Manoj P.K., Structural, electrical and optical studies on chemically deposited tin oxide films from inorganic precursors, Materials Chemistry and Physics, 2005, 93,194–201.
18. Patil L.A. , Shinde M.D., Bari A.R., Deo V.V., Synthesis of $SnO_2$ hollow microspheres from ultrasonic atomization and their role in hydrogen sensing, Materials Science and Engineering B, 2011,176, 579–587.
19. Salunke R. R., Lokhande C. D., Effect of film thickness on liquefied petroleum gas (LPG) sensing properties of SILAR deposited CdO thin films, Sensors and Actuators B, 2008,129, 345-351.
20. Jain G. H., Patil L.A., CuO- doped BSST thick films resistors for ppb level $H_2S$ gas sensing at room temperature, Sensor and Actuators B, 2007,123,246-253.
21. Jain G. H., Patil L.A., Wagh M. S., Patil D. R., Patil S. A., Amalnerkar D. P., Surface modified $BaTiO_3$ thick film resistors as $H_2S$ gas sensors, Sensor and Actuators B, 2006, 117, 159-165.
22. Patil L. A., Suryawanshi D. N, Pathan I. G. and Patil D. G., Effect of variation of precursor concentration on structural, microstructural, optical and gas sensing properties of nanocrystalline $TiO_2$ thin films prepared by spray pyrolysis techniques, Bull. of Mater. Sci., 2013,3, 1153–1160.
23. Kolmakov A., Klenov D. O., Lilach Y., Stemmer S., Moskovits M., Enhanced gas sensing by individual $SnO_2$ nanowires and nanobelts functionalized with Pd catalyst particles, Nano. Lett., 2005,5, 667–673.
24. Vlasov Y., Bratov A., Levichev S., Tarantov Y., Enzyme semiconductor sensor based on butyrylcholinesterase, Sensor and Actuators B Chem., 1991,4, 283–286.

**✳✳✳✳✳**